Rakenteiden Mekaniikka (Journal of Structural Mechanics)
Vol. 58, No. 4, 2025, pp. 155–173
https://rakenteidenmekaniikka.journal.fi/index
https://doi.org/10.23998/rm.152288

VERTAISARVIOITU
KOLLEGIALT GRANSKAD
PEER-REVIEWED
www.tsv.fi/tunnus

Transient thermal stress FE-analysis method development

Sami Kreivi[1], Janne Kemppainen, Teemu Kuivaniemi, Antti-Jussi Vuotikka and Tero Frondelius

Summary This research paper addresses the challenges of thermomechanically loaded components in four-stroke medium-speed engines, focusing on exhaust pipe failures due to low-cycle thermal fatigue. Wärtsilä's shift towards 100% renewable energy has altered engine operating conditions, leading to new challenges in exhaust components subjected to fluctuating thermal conditions. The study focuses on the transient method's ability to detect phenomena during heating and cooling in stress and temperature histories, optimizing the transient analysis definitions and providing some principles for design modifications in thermal stress problems. A case study of nodular cast iron exhaust manifold is used as an example. Traditional methods using cyclic steady-state temperatures have been found insufficient, prompting the development of a more accurate transient method that uses measured temperatures during the engine's thermal cycle. The paper compares conventional steady state heat transfer analysis and two transient heat transfer analyses for defining thermal boundary conditions. The temperatures in the first transient analysis are defined accurately from the measurements, leading to more realistic results and long calculation time. The second transient analysis is improved to offer a balanced method between accurate thermal boundary definitions and shorter calculation time. The transient method reveals higher stress amplitudes in previously low-stress zones, identifying the actual critical points on the exhaust pipe.

Keywords: transient, thermal stress, medium-speed four-stroke engine, low-cycle thermal fatigue

Received: 29 November 2024. Accepted: 23 June 2025. Published online: 27 October 2025

Introduction

Wärtsilä has actively contributed to the energy transition towards the 100% renewables future by developing its products and creating strategies for how this target could be achieved as soon as possible [1]. This includes the usage of engine power plants to balance the energy system when renewable energy is not enough to fulfil the needs of consumption. In practice, the usage of engines has tilted from the old base load provider to peak facilities which means that previously engines would run, for example, two weeks with one start whereas now the engines may be started 20 times in the same period and run only hours per start. As a result, the change in engine operating conditions has led to locating cracks (see Figure 1) in the exhaust components that have not had problems before, nor the simulations have pointed out.

[1]Corresponding author: sami.kreivi@gbw.fi

Figure 1. Low-cycle thermal fatigue caused exhaust support failure.

The dominant failure mode that has become more significant along this change in engine usage is low-cycle thermal fatigue (LCTF). Low-cycle thermal fatigue is a critical consideration in the performance and durability of components subjected to cyclic thermal loading, especially in environments characterized by start-stop cycles and fluctuating operational conditions [2, 3]. The conventional workflow of using cyclic steady-state temperature fields in fully heated up and cooled down states of the engine has proven to be insufficient for a reliable thermal stress analysis. On the other hand, simulating full transient thermal cycles which match measurement data usually leads to time-consuming and cost-heavy calculations. Due to this, an intermediate solution was needed. The cost-effective simulation process is a relevant issue in designing thermomechanically loaded engine components due to the number of design iterations required for the final product. Design optimization usually takes several simulations with critical geometry modifications to reach the desired resolution, as the interaction of thermal and mechanical loads in a multi-component assembly is not always so predictable.

This paper focuses on a case study of a nodular cast iron (EN-GJS-500-14) exhaust manifold in a four-stroke medium-speed engine to investigate the effects, methods and simulation workflows for LCTF in an extensive range of temperature changes. The conventional and improved simulation methods are explained with some comparisons considering the total simulation times and reliability of the results. In addition, some simple design principles for thermomechanically loaded structures and acceptance criteria regarding cyclic thermal stresses are presented.

Low-cycle thermal fatigue in engine components

Fatigue in metals is conventionally considered as the consequence of highly localized cyclic inelastic deformation that requires thousands or even millions of cycles to initiate and propagate a crack to a macroscopic scale. The regime of low-cycle fatigue, however, emphasises greater and more homogeneously distributed inelastic deformation that leads to crack initiation and propagation at clearly lower amount of load cycles (approximately

less than 10^4 cycles). In an environment of great temperature changes, the more important condition called thermal fatigue is imparting low-cycle endurance as the cyclic deformation is caused by temperature gradients leading to thermal expansion in the frequency of heating and cooling [2].

When a component subjected to cyclic heating and cooling is in a mechanically restricted state, often bolted to a larger assembly, the overall loading derives from phases of mechanical and thermal loads [3]. The exhaust manifold of the case study is a good example in these situations as the exhaust gases heat the channels and their nearest surroundings of the manifolds to over 550 °C. In contrast, the temperatures of the bracket or block on which the manifold is bolted stay under 100 °C on steady-state full load temperatures. This leads to non-uniform thermal expansion of the exhaust manifold, which again amplifies the multiaxial stress state. Figure 2 represents the absolute maximum principal stresses and temperatures of hot and cold points on adjacent components during a typical thermal cycle. As a result of this stress state, the first thermal load cycles often lead to plastic deformation in localized high-stress zones where the material's yield point is exceeded [3]. Residual stresses that occur in these high-stress zones create high stress amplitudes, as the stress is reversed from tension to compression or vice versa in the cooling phase of the engine.

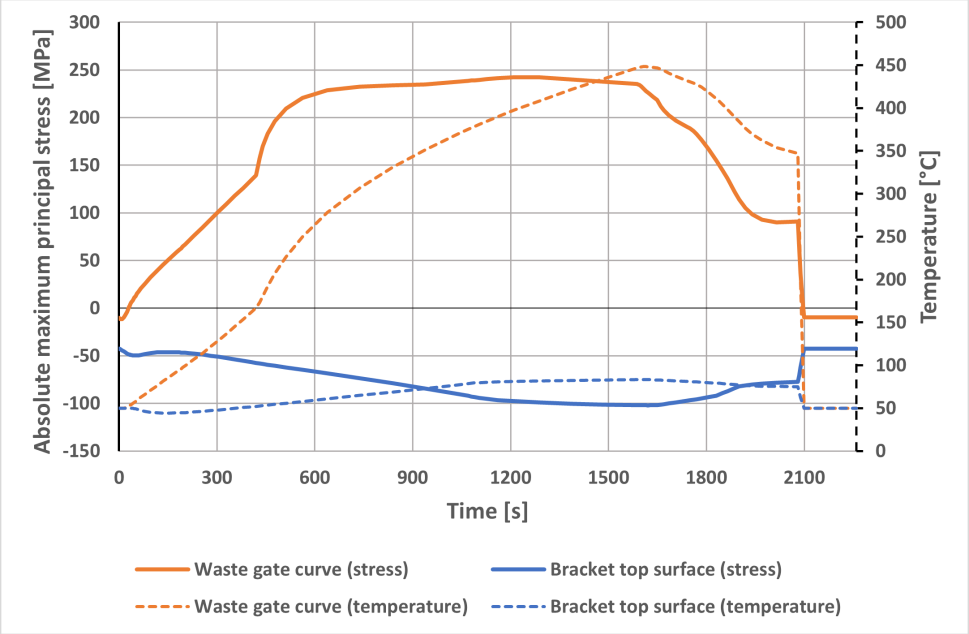

Figure 2. Absolute maximum principal stress and temperature of adjacent hot and cold engine components during a typical thermal cycle.

In the context of ductile iron, which is frequently used in thermomechanically loaded components, knowledge about material properties at intermediate temperatures is demanded for accurate lifetime predictions in challenging operating conditions. The mechanical properties of ductile irons with elevated silicon contents have proven advantageous suitability for engine components due to their higher strength and ductility, allowing significant weight reduction in the final casting [4, 5]. Increased pearlite fraction in the microstructure and silicon content of the ferritic structure increases the tensile and yield strength properties of the material at temperatures ranging from room temperature to 450 °C [6]. Material models based on measurements at intermediate temperatures provide

valuable tools for applications such as Finite Element Method (FEM) calculations and the optimization of thermomechanically loaded ductile iron components.

In addition to material characteristics, the geometry shape of the component under the cyclic thermal loading also significantly affects LCTF performance, and multiaxial thermal fatigue is more destructive than isothermal fatigue [7]. Generally, the material property data from material experiments, temperature data from laboratory engine tests and geometrical shapes proposed by component experts and designers are combined in numerical simulations of thermomechanically loaded engine components. The vast amount of variables and situation-dependent conditions should be limited so that the causes of possible failures, the solutions to overcome them, and the overall conclusion if the component is applicable in the conditions it is designed for could be understood via simulations within a tight schedule. Another focus of this paper is the method development of the simulation process and guidelines on the design characteristics of thermally loaded engine components as a part of continuous development in simulation-enhanced product improvement [8].

As in [9, 10], the optimization of structure design is one of the most effective approaches in LCTF problems and even minimal appropriately chosen modifications in geometry can have a huge impact on the feasibility of a component [11]. Thermal stress amplitudes are highly prone to develop in sharp shapes and areas that experience a wide range of temperatures and uneven changes in temperature distributions. Adding stiffening brackets or ribs, removing unnecessary material for improved flexibility of thermal expansion, and enlarging the radius in critical locations have relatively significant effects in these situations [9]. However, the communication between the structural analysts, designers and casting experts must be seamless for a final design that meets the design requirements. In addition to the component's required lifetime, the requirements of manufacturability from casting moulds and machining to the final installation on the engine assembly must also be met. Manually redesigning the component and obtaining the effects of the modifications with an FE-analysis naturally takes a lot of time in the design process. This has led to rising attention towards geometric deep learning methods for predicting the results of analyses without running the actual cost-heavy calculations [12]. Getting a prediction of stress distribution with a slightly modified geometry and the same loading in a shortened time would give valuable insights into the redesign, thus shortening the overall time of the design process.

LCTF is not a new problem in the industry and various methods have been developed to estimate the crack initiation and lifetime of thermomechanically loaded structures [13, 14, 15]. The emphasis on thermomechanical fatigue simulations has traditionally been prioritized towards more operating-critical components such as cylinder heads and combustion-related components [16, 17]. In the automotive industry, the low-cycle fatigue phenomenon is known to be the most common cause of exhaust manifold failure [18, 9] and several stress- and strain-based multiaxial fatigue life estimation models have been developed [14]. Lorenzini et al. [18] used the equivalent plastic strain range registered for a single thermal cycle (ΔPEEQ) as a key factor to estimate the fatigue lifetime based on the research done by Chen et al. [19], where they studied the thermomechanical behaviour of an exhaust manifold for a turbocharged gasoline engine and proposed a plastic deformations-based methodology to simulate the structural failure. The deformation-based methodologies seem to offer a valid possibility alongside the traditional stress-based theories in the regime of low-cycle thermal fatigue phenomenon which must be studied in the future also with the usage of large-bore medium-speed engines. However, the focus

of this paper is on the transient thermal stress simulation process as stated and thus, the fatigue lifetime evaluation is not emphasized as such.

Conventional steady state model (SS)

The heat transfer analysis with FEM is a computational technique employed to predict the distribution of temperature within a solid body subjected to various thermal loads and boundary conditions. As an uncoupled heat transfer analysis, in this case, the stress or deformation of solid bodies is not considered. In a conventionally used steady-state analysis, the system reaches a thermal equilibrium where the temperature distribution is not time-dependent. Key aspects of the uncoupled steady-state heat transfer FEM analysis procedure include mesh generation, material properties assignment, thermal and mechanical boundary condition specification, and solution convergence. The relatively simple and quick process of two FEM analyses in this conventional method is crucial when several iterations might be needed to find the optimum design. In the case study of this paper, Abaqus/Standard 2023.HF2 [20] was used as a FEM-solver and fe-safe 2023 Hot Fix 2 [21] was used for critical plane analysis. Stress amplitudes and mean stresses on maximum normal stress planes were solved only to discover the most critical points of the design. The studied exhaust pipe assembly and its main components can be seen in Figure 3.

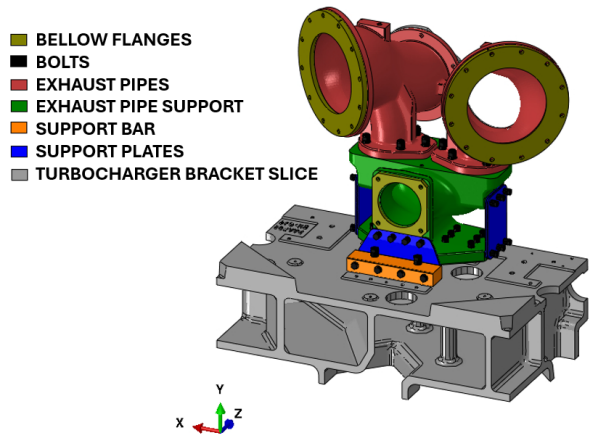

Figure 3. Exhaust pipe assembly FE-model.

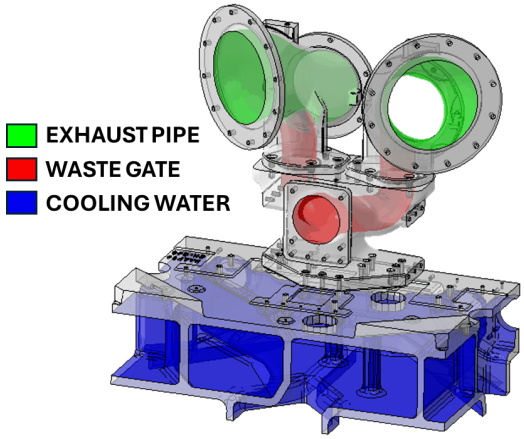

Figure 4. Convection surfaces of the FE-model.

Conventionally the thermomechanical problems have been mainly solved by examining the stress states inflicted by the maximum fluid temperatures (e.g. exhaust gas, cooling water, charge air), which are generally well-known for several locations in the studied assemblies. Additionally, for thermomechanical fatigue problems, the cyclic load could be obtained from the difference of stress states in extreme temperatures. In the case of base-load-providing engines, these have been sufficient and cost-effective methods to evaluate the feasibility of component designs, as the temperature fields were calculated with a steady-state heat transfer analysis. The convection from fluids to solids in heat transfer was defined as surface-based films (*SFILM [20]) for predefined surfaces of the FE-model shown in Figure 4. The heat flux $q_{convection}$ for the surface-based films is governed by Newton's cooling law [22] using the given film coefficient h, solid surface temperature T_s and the reference fluid temperature T_f

$$q_{convection} = h \cdot (T_s - T_f). \tag{1}$$

Conductive heat flux $q_{conduction}$ in the solid material is calculated according to Fourier's conduction law (here as one-dimensional for simplicity) [22] with the thermal conductivity of the solid material k and the temperature gradient dT/dx

$$q_{conduction} = -k \cdot \frac{dT}{dx}. \tag{2}$$

Heat transfer rate Q is obtained from the sum of the heat fluxes multiplied by their respective areas of effect A

$$Q = q_{convection} \cdot A_{convection} + q_{conduction} \cdot A_{conduction} \tag{3}$$

and in a steady-state equilibrium, the heat transfer rate is zero everywhere (Q = 0). A sequentially coupled thermal stress analysis can be performed using the temperature field from the heat transfer analysis as a thermal load.

The thermal boundary conditions (TBC) used in the conventional steady-state heat transfer analysis (SS) of the case study are shown in Tables 1, 2 & 3, in which only the final temperatures for every condition during the thermal cycle were taken from measurements. The film coefficients for SS were tuned during a sensitivity study so that the temperatures in measured points in the steady state would match simulations. In the sequentially coupled thermal stress analysis, mechanical loads such as bolt pretension forces and pressures during the thermal cycle were applied to the structure in addition to the temperature fields, and the FEM predicted the distribution of stress and deformation under a combination of thermal and mechanical loads.

Table 1. Thermal boundary conditions for exhaust pipe in SS.

Step	Duration [s]	Temperature [°C]	h [kW/(m^2·°C)]
Preheat (steady state)	1	0 - 50	300
Full load (steady state)	100	50 - 580	450
Cool down (steady state)	100	-	-

Table 2. Thermal boundary conditions for waste gate in SS.

Step	Duration [s]	Temperature [°C]	h [kW/(m^2·°C)]
Preheat (steady state)	1	0 - 50	150
Full load (steady state)	100	50 - 580	300
Cool down (steady state)	100	-	-

Table 3. Thermal boundary conditions for cooling water in SS.

Step	Duration [s]	Temperature [°C]	h [kW/(m^2·°C)]
Preheat (steady state)	1	0 - 50	5000
Full load (steady state)	100	50 - 82	5000
Cool down (steady state)	100	50	5000

The material of the greatest interest in the case study of this paper is EN-GJS-500-14 [23], for which a temperature-dependent elastoplastic material model with perfect J2-plasticity was created for FEM simulation purposes (see Figures 5 & 6). Thermal conductivity and thermal expansion coefficient were also defined with temperature-dependent values, as shown in Figures 7 & 8. Density of 9.6 g/cm^3 and Poisson's ratio of 0.29 were set as constants for the material model. The fatigue limit of EN-GJS-500-14 in elevated temperatures was not found in an extensive literature review [24, 25], and no fatigue tests of Wärtsilä's own were performed at the time of this study. Due to their close to similar microstructures, it was presumed that the fatigue limit of EN-GJS-500-14 was in the same range as in EN-GJS-500-7 with 50 % pearlite, for which there was accessible fatigue test data in higher temperatures. In addition, according to the European Standard of spheroidal graphite cast irons, the fatigue strength of EN-GJS-500-14 should be at least as high as the fatigue strength of EN-GJS-500-7 at room temperature [23].

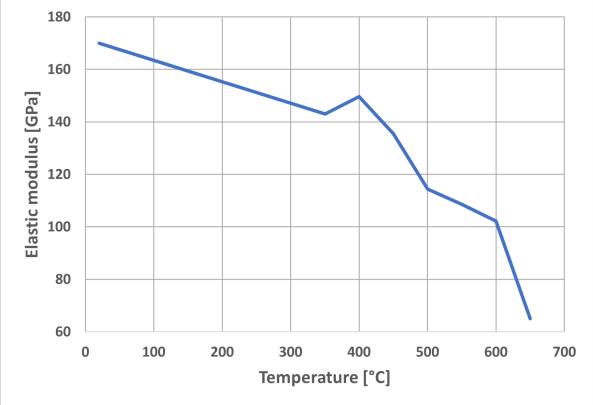

Figure 5. Temperature-dependent elastic modulus of EN-GJS-500-14 material model.

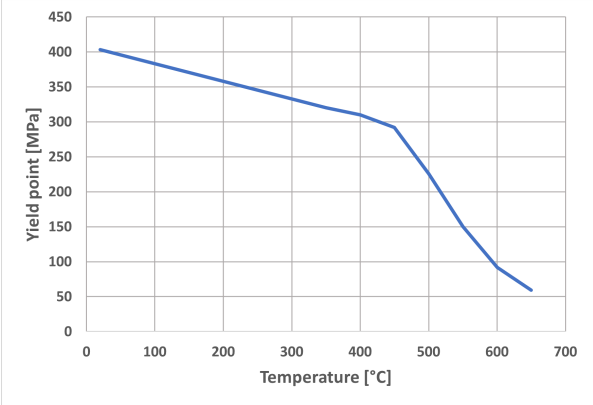

Figure 6. Temperature-dependent yield point of EN-GJS-500-14 material model.

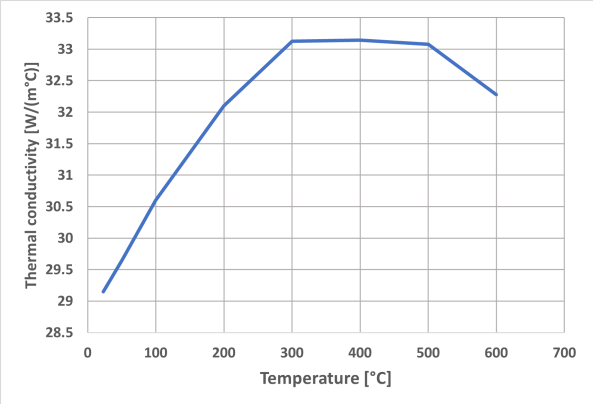

Figure 7. Temperature-dependent thermal conductivity of EN-GJS-500-14 material model.

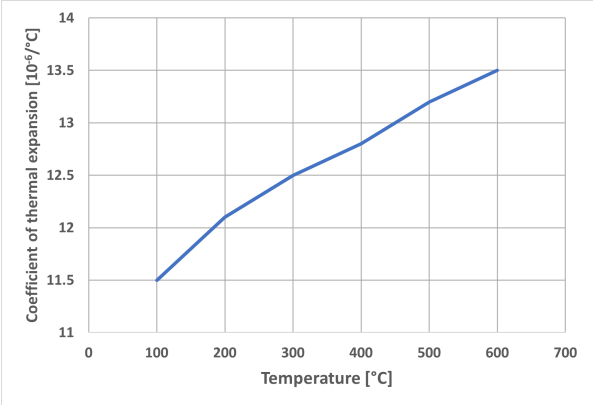

Figure 8. Temperature-dependent coefficient of thermal expansion of EN-GJS-500-14 material model.

Figure 9 shows the stress-life (SN) curve of EN-GJS-500-7 generated from the fatigue tests in 450 °C. A target life of 10^4 cycles was selected for the studied LCTF problem, for which a fatigue limit of circa 1.31 can be read from the SN-curve. However, to account for the uncertainty of using the fatigue limit from not exactly matching material and

to add safety to simulation results, a safe limit for stress amplitudes in EN-GJS-500-14 during the thermal cycle was selected as 1.0. In this paper, this value is used for the normalization of stress results. Regarding the detrimental effect of tensile mean stress for fatigue, the limit of stress value 1.0 was strict under tensile mean stress, but for points under compressive mean stress, an amplitude of 1.15 was accepted [26].

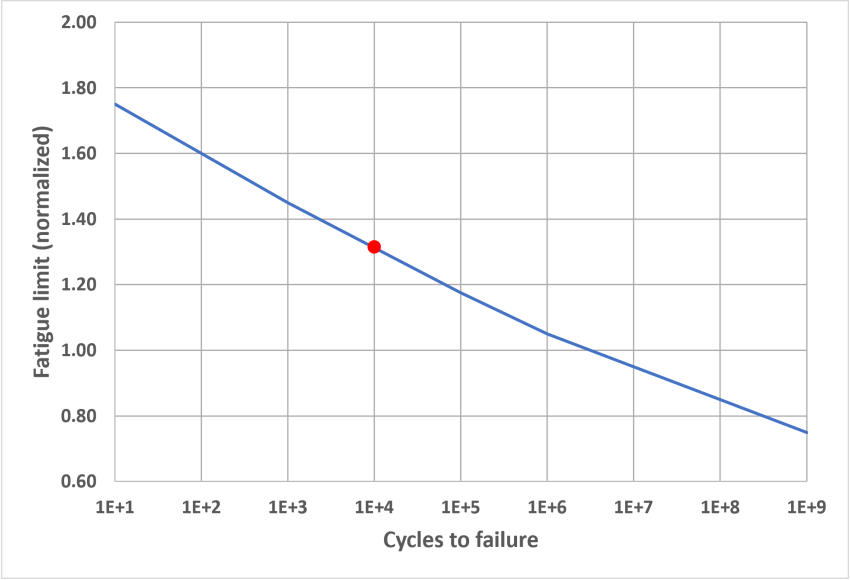

Figure 9. SN-curve for EN-GJS-500-7 (50% pearlite) in 450 °C.

Transient model (T1)

The analysis type must be altered to consider the phenomena during the heating and cooling, not merely at the steady states when the target temperatures are reached in the entire assembly. Sequentially coupled stress analysis with thermal loads from steady-state heat transfer analysis can examine the solid component's deformation and stress state as a function of linearly changing temperature, i.e. the final state after perfectly uniformly developed temperatures. However, due to the usage profile change, the non-linearly developing temperature field during the thermal cycle was needed as input to the stress analyses. This was possible by obtaining the temperatures from transient heat transfer analysis, which solves the time-dependent thermal field [27]. In transient heat transfer analysis, Abaqus solves the developed thermal field implicitly at every time increment with backward Euler time integration method. Approximation for the next state y_{k+1} in the backward Euler method is obtained as a sum of the previous state y_k and the function $f(t_{k+1}, y_{k+1})$ multiplied with the time step Δt

$$y_{k+1} = y_k + \Delta t \cdot f(t_{k+1}, y_{k+1}), \tag{4}$$

where t_{k+1} is the total time at the next state [28]. The function f and the initial state $y(t_0) = y_0$ must be known. Analysis steps are defined regarding the thermal boundary conditions and the heat transfer equations are solved with the components' material properties. Additional thermophysical material properties in the transient heat transfer rate equation are the specific heat capacity c_p and density ρ, which are defined as a function of temperature [29]. Now the heat transfer rate can be set as equal to Equation 3 with

the rate of temperature change dT/dt and the thermal diffusivity α, which describes the heat transfer rate inside the material

$$Q = \frac{1}{\alpha} \cdot \frac{dT}{dt} = \frac{\rho \cdot c_p}{k} \cdot \frac{dT}{dt}. \tag{5}$$

Gathering the temperatures of fluids like exhaust gas and cooling water for the whole thermal cycle is an essential part of the transient heat transfer analysis. These are usually collected from measurements, and possibly even from collected field data. The more challenging task is to find out the film coefficients for different fluids and mass flow rates without separate computational fluid dynamics (CFD) analyses. In this study, the film coefficients were inferred with a sensitivity study comparing measured and simulated temperatures in an exhaust pipe assembly. Film coefficients for hot and cool exhaust gas with a high mass flow rate (main exhaust pipe channels), hot and cool exhaust gas with a low mass flow rate (waste gate channels) and one film coefficient for circulating cooling water were found. Some future research for a workflow including a coupled CFD-FEM thermal stress analysis [30] in finding a more realistic thermal field over the whole thermal cycle should be conducted, but the current methods were concluded sufficient to aid the design process of increasing the lifetime of thermomechanically loaded components.

The initial efforts after the change of heat transfer analysis type from steady state to transient led to rather detailed thermal boundary conditions. Thermal boundary conditions for the heat transfer analysis of an accurate one-way coupled transient thermal stress analysis (T1) are listed in Tables 4, 5 & 6. These temperatures were picked from the measurement data whenever a significant change occurred in either engine speed or load level, and the duration of a single temperature change could be as short as 20 seconds. The preheating step is needed only before the first thermal cycle to reach the initial thermal state of the simulated assembly. Although realistically there are not any exhaust gases flowing in the exhaust pipes during the preheating, defining exhaust gases to rise to preheat temperature during it will help the FEM solver to reach a steady state. The same principle can be used for the last cool down step.

Table 4. Thermal boundary conditions for exhaust pipe in T1.

Step	Duration [s]	Temperature [°C]	h [kW/(m^2·°C)]
Preheat (steady state)	1	0 - 50	300
Engine speed 1	30	50 - 200	300
Engine speed 2	20	200 - 203	300
Engine speed 3	135	203 - 270	300
Engine load 1	235	270 - 440	300
Engine load 2	650	440 - 525	450
Engine load steady	520	525 - 580	450
Engine load off 1	20	580 - 545	450
Engine load off 2	40	545 - 530	450
Engine load off 3	100	530 - 520	300
Engine load off 4	80	520 - 375	300
Engine speed off	70	375 - 265	300
Engine cooling	180	265 - 360	300
Cool down (steady state)	100	-	-

Table 5. Thermal boundary conditions for waste gate in T1.

Step	Duration [s]	Temperature [°C]	h [kW/(m^2·°C)]
Preheat (steady state)	1	0 - 50	150
Engine speed 1	30	50 - 200	150
Engine speed 2	20	200 - 203	150
Engine speed 3	135	203 - 270	150
Engine load 1	235	270 - 440	150
Engine load 2	650	440 - 525	300
Engine load steady	520	525 - 580	300
Engine load off 1	20	580 - 545	300
Engine load off 2	40	545 - 530	300
Engine load off 3	100	530 - 520	150
Engine load off 4	80	520 - 375	150
Engine speed off	70	375 - 265	150
Engine cooling	180	265 - 360	150
Cool down (steady state)	100	-	-

Table 6. Thermal boundary conditions for cooling water in T1.

Step	Duration [s]	Temperature [°C]	h [kW/(m^2·°C)]
Preheat (steady state)	1	0 - 50	5000
Engine speed 1	30	50	5000
Engine speed 2	20	50 - 40	5000
Engine speed 3	135	40 - 45	5000
Engine load 1	235	45 - 55	5000
Engine load 2	650	55 - 82	5000
Engine load steady	520	82	5000
Engine load off 1	20	82	5000
Engine load off 2	40	82 - 80	5000
Engine load off 3	100	80 - 78	5000
Engine load off 4	80	78 - 75	5000
Engine speed off	70	75 - 72	5000
Engine cooling	180	72	5000
Cool down (steady state)	100	50	5000

Improved transient model (T2)

A simplified method for defining thermal boundary conditions for the full thermal cycle was developed by examining the phases of heating and cooling that had a distinguishable effect on the thermal stresses, as the stress response to fast, short-term changes in temperature would be very minimal in solid components. The transient step durations did not need to be shorter than 60 seconds, and the duration of the steady state cool down step was defined as 100 seconds only for the sake of easier results analyzing. The improved one-way coupled transient thermal stress analysis (T2) included only the phases for engine start and load, followed by a shut down of the engine and a final steady state cool down (see Tables 7, 8 & 9). The main differences in this approach were to reduce the number of analysis steps into more general engine running phases, and to follow the

temperatures of the fluids in convective channels, not the measured temperatures of the solid components.

Exhaust gas temperatures needed as inputs for T2 are the initial exhaust gas temperature right after the engine is started (here 200 °C), the temperatures at the start (480 °C) and the end of the loading phase (580 °C, maximum temperature) and at the time of the engine being completely shut down (265 °C). In addition, the film coefficient for cool exhaust gas is used in every step apart from the highest load step, when the film coefficient for hot exhaust gas is more suitable. The thermal stresses were simulated as a sequentially coupled thermal-displacement analysis with the additional mechanical loads as in the steady-state method, but the step times were defined regarding the steps in the used heat transfer analysis.

Table 7. Thermal boundary conditions for exhaust pipe in T2.

Step	Duration [s]	Temperature [°C]	h [kW/(m^2·°C)]
Preheat (steady state)	1	0 - 50	300
Start	420	200 - 480	300
Load	1200	480 - 580	450
Shut down	300	580 - 265	300
Cool down (steady state)	100	50	300

Table 8. Thermal boundary conditions for waste gate in T2.

Step	Duration [s]	Temperature [°C]	h [kW/(m^2·°C)]
Preheat (steady state)	1	0 - 50	150
Start	420	200 - 480	150
Load	1200	480 - 580	300
Shut down	300	580 - 265	150
Cool down (steady state)	100	50	150

Table 9. Thermal boundary conditions for cooling water in T2.

Step	Duration [s]	Temperature [°C]	h [kW/(m^2·°C)]
Preheat (steady state)	1	0 - 50	5000
Start	420	50 - 82	5000
Load	1200	82	5000
Shut down	300	82 - 72	5000
Cool down (steady state)	100	50	5000

Results

In Figure 10 can be seen the normalized absolute maximum principal stress and temperature of a critical point (see Figure 11) in the studied exhaust pipe during a thermal cycle in SS. Step duration acts only as a kind of scale factor for the temperature fields

that should be achieved at the end of a step, and thus the time scale is not physically meaningful in a steady-state analysis. The main drawback of this method is that only the stress states deriving from the fully developed and fully cooled down thermal field can be seen, there is not any stress history in between. Naturally, the maximum stresses in maximum temperatures and residual stresses in a cooled-down state can be collected, but these values do not tell the whole truth or if the critical point found with this method is the actual critical point in the structure.

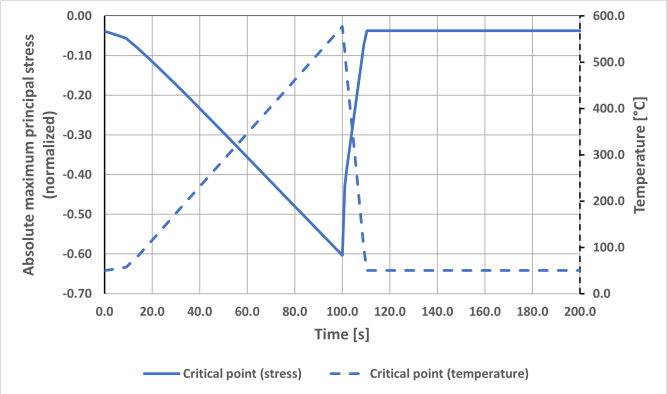

Figure 10. Absolute maximum principal stress (normalized) and temperature of the critical point in SS.

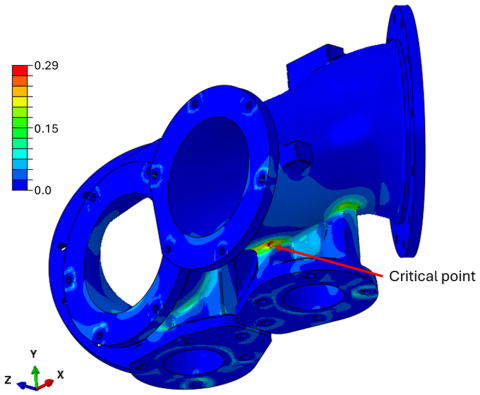

Figure 11. Normalized stress amplitude field and the critical point in SS.

The transient method's capability of noticing the phenomena during the heating and cooling is seen in absolute maximum principal stress and temperature history diagrams presented in Figure 12. Bluntly, the absolute maximum principal stress on the critical point ascends on the tensile side during the engine start and the beginning of loading but descends to circa two-thirds from a fully reversed compressive stress during the end of loading and shutdown steps. On the steady-state cooldown step, the stress reaches a magnitude of near zero.

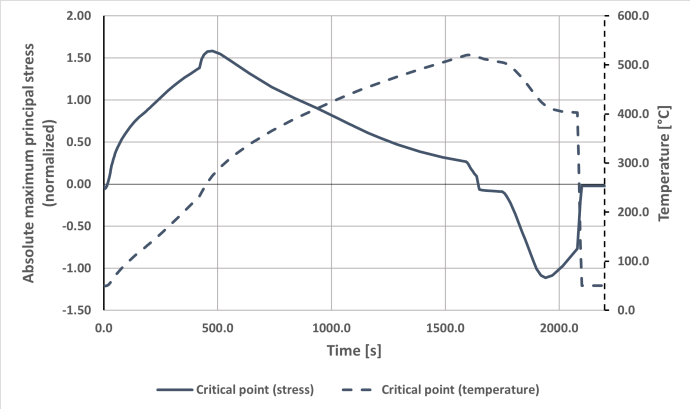

Figure 12. Absolute maximum principal stress (normalized) and temperature of the critical point in T1.

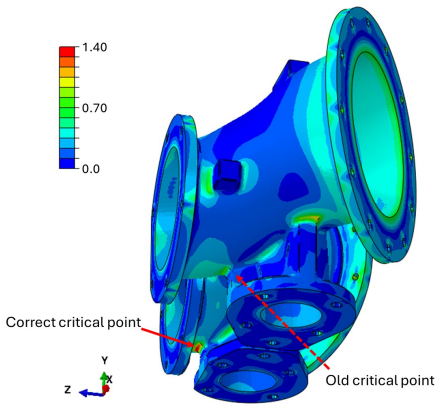

Figure 13. Normalized stress amplitude field and the critical point in T1.

The stress amplitude field from the second thermal cycle of T1 can be seen in Figure 13. The most noteworthy change in transient simulation results compared to the prior steady-state simulation results is the significantly higher stress amplitudes in locations that were nearly zero-stress zones. The new and correct critical point is even on the

other exhaust pipe than the prior critical point. The absolute maximum principal stress amplitude during the second thermal cycle with the T1 thermal boundary conditions reached a stress value of 1.35.

Comparing the stress and temperature history diagrams from T1 and T2 (Figure 14), the main difference is the amount of details in variation. As the stress amplitude distribution is the primary variable needed for efficient modification of the geometries to find feasible designs, the lack of details in stress history apart from the extreme values is not a problem. The time saved in the simulation is an asset of greater value, which justifies the use of simplified thermal boundary conditions during the product development process. The difference in the stress amplitude fields resulting from T1 and T2 is minimal and the critical point is located in the same rounding below the smaller flange.

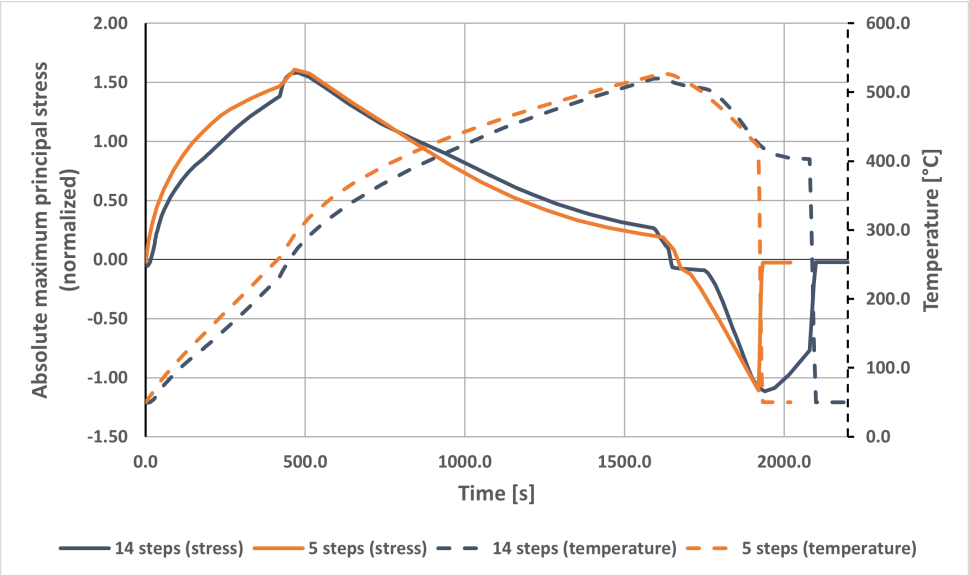

Figure 14. Absolute maximum principal stress (normalized) and temperature of the critical point with T1 (14 steps) and T2 (5 steps).

Table 10. Comparison of calculation times with different approaches.

Method	Calculation time [h]			
	Unique TBC definitions	Heat transfer analysis	Stress analysis	Critical stress amplitude (norm.)
SS (2 cycles)	3	0.4	6.7	0.283
T1 (2 cycles)	14	3.1	18.7	1.349
T1 (3 cycles)	14	3.1	29.1	1.348
T2 (2 cycles)	5	1.8	13.5	1.358

A comparison of calculation times between the SS, T1 and T2 thermal boundary conditions (Table 10) shows fundamental differences in the approaches explained in this paper. The conventional method SS, including only the steady state thermal boundary conditions of preheating, full load and cool down, is the most time-efficient approach but does not fully reveal the stress states of the studied component during a realistic thermal cycle. The most accurate approach T1, which has transient thermal boundary conditions

defined in detail following the slightest changes in engine speed or load level, leads to rather heavy and time-consuming calculations. Especially the sequentially coupled stress analyses proved long, reaching calculation times of over 9 hours per thermal cycle. On the other hand, the critical stress amplitudes obtained from this method can be considered the most accurate regarding the available input data. The improved T2, which includes the main transient thermal boundary conditions from the detailed definitions, can be seen as a compromise between the SS and T1, leading to rational stress results and reasonable calculation time. For the case study in this paper, it can be noticed that additional thermal cycles after two cycles do not lead to added value regarding stress results. Thus it can be concluded that the plastic deformation with the applied loads has fully developed during the first thermal cycle, and the stress results collected from the second cycle are reliable for feasibility examination.

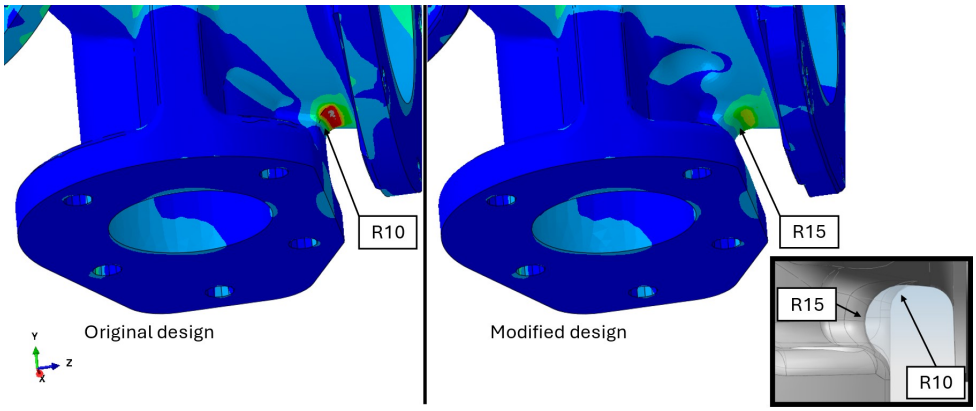

Figure 15. Stress amplitude fields in original and modified exhaust pipe designs.

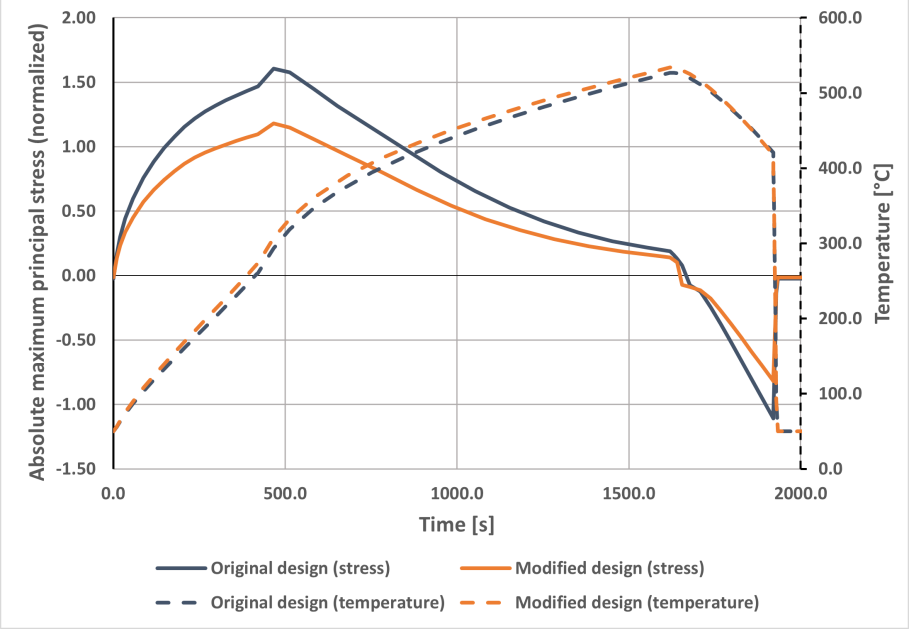

Figure 16. Absolute maximum principal stress (normalized) and temperature of the critical point in T2 with the original and modified exhaust pipe.

Simple geometric modifications were applied to the critical locations of the original exhaust pipe assembly to reach acceptable stress amplitude limits. Figure 15 shows the

most significant geometrical modification and effects in the stress amplitude field in the area of the critical point of the exhaust pipe. By enlarging the radius of the rounding from R10 to R15 and lightening the material from the rib below the flange the stress range deriving from thermal expansion during the thermal cycle can efficiently be decreased. The effect of local geometrical optimization near the critical point can be seen in Figure 16. While the thermal cycle of the critical point remains, the lesser restriction of thermal deformation results in a drop of the stress amplitude from 1.35 to 1.0 which can be considered acceptable.

Discussion

Field reports of crack failures in locations of exhaust pipe components where problems had not occurred before nor simulations pointed out launched a study considering new challenges related to low-cycle thermal fatigue in large-bore four-stroke medium-speed engines. In this study, the simulation methods for these new thermal stress challenges, particularly in cast iron exhaust components, emerging along the change in power plant engines' usage profile were developed further and demonstrated using a case study of a nodular cast iron exhaust manifold. The main goals of the study were to find a suitable workflow for simulating components under vastly fluctuating thermomechanical conditions and to bluntly illustrate some simple design modification principles for the most critical components.

The drawbacks of conventional steady-state heat transfer analysis in the studied application were pointed out and the costly but more accurate method of transient heat transfer analysis was improved, resulting in significantly shorter calculation times. Practically the design process might require numerous geometrical optimization iterations until structurally functional and durable designs, which are also realistic to manufacture, are found. Here the importance of lightened calculation and shorter analysis times can be emphasized. A comparison of the results of conventional (SS), accurate (T1) and improved (T2) workflow in the case study assembly showed that the most critical stress amplitude locations might not be visible at all with the steady-state thermal cycles. On the other hand, the improved transient thermal cycle definition revealed the same stress history as the accurate definition in a much shorter calculation time. Simple but effective geometrical modifications, such as enlarging the rounding radius and slightly removing material from the critical location, were applied to the studied EN-GJS-500-14 exhaust manifold to decrease the highest stress amplitude during the thermal cycle from the value of 1.35 to 1.0. The decreased stress amplitude value of 1.0 was considered safe for low-cycle thermal fatigue based on the SN-curve of a material with close to similar microstructure, regarding the uncertainties with a safety margin in the fatigue limit.

Even though the improved workflow developed during the study firstly led to more realistic results and secondly shortened the analysis times remarkably, along with the acquired knowledge of the effective geometrical modifications, there are still many aspects of thermal stress simulations with viable future research. Naturally, fatigue tests in target conditions for the studied materials would provide precise information for a basis for the material model to be used in simulations. Additionally, the deformation-based acceptance criteria used more in thermal problems in the automotive industry might also be feasible in large-bore engines as an alternative to stress-based criteria. A coupled CFD-FEM analysis could prove useful, especially in capturing the realistic thermal field as a function of time to be utilized in stress analysis. Finally, taking advantage of the con-

stantly evolving contemporary deep-learning strategies might shorten the overall design process times with the ability to predict the stress distribution in a modified geometry without the need for a full cost-heavy calculation. These areas of uncertainty or possible added value regarding the subject would suggest listing fatigue tests of EN-GJS-500-14 in a temperature range of 100...600 °C, added with more in-depth method development studies of deformation-based acceptance criteria for thermomechanical problems, coupled CFD-FEM heat transfer analyses and physics-informed machine-learning algorithms for geometry optimization as the primary subjects for future research.

Acknowledgement

Funded by the European Union (Grant Agreement No. 101058179; ENGINE). Views and opinions expressed are however those of the authors only and do not necessarily reflect those of the European Union or the European Health and Digital Executive Agency. Neither the European Union nor the granting authority can be held responsible for them.

References

[1] Wärtsilä. Towards a 100% renewable energy future, 2024. Last accessed 8 February 2024. URL: https://www.wartsila.com/docs/default-source/power-plants-documents/downloads/presentation/towards-a-100-renewable-energy-future---presentation.pdf?sfvrsn=914a2a44_8.

[2] G.R. Halford. *Low-cycle thermal fatigue*, volume 87225. Lewis Research Center, 1986.

[3] S.N. Lekakh, M. Buchely, R. O'Malley, L. Godlewski, and M. Li. Thermo-cycling fatigue of SiMo ductile iron using a modified thermo-mechanical test. *International Journal of Fatigue*, 148:106218, 2021. doi:10.1016/j.ijfatigue.2021.106218.

[4] C. Hartung, E.G. Hoel, E. Ott, R. Logan, A. Plowman, and D. Wilkinson. Research on solution strengthened ferritic ductile iron (SSFDI) structure and properties using different treatment and inoculation materials. *International Journal of Metalcasting*, 14(4):1195–1209, 2020. doi:10.1007/s40962-020-00469-4.

[5] D. Franzen, B. Pustal, and A. Bührig-Polaczek. Influence of graphite-phase parameters on the mechanical properties of high-silicon ductile iron. *International Journal of Metalcasting*, 17(1):4–21, 2023. doi:10.1007/s40962-022-00761-5.

[6] J. Laine, K. Jalava, J. Vaara, K. Soivio, T. Frondelius, and J. Orkas. The mechanical properties of ductile iron at intermediate temperatures: The effect of silicon content and pearlite fraction. *International Journal of Metalcasting*, 15:538–547, 2021. doi:10.1007/s40962-020-00473-8.

[7] A. Fissolo, S. Amiable, O. Ancelet, F. Mermaz, J. M. Stelmaszyk, A. Constantinescu, C. Robertson, L. Vincent, V. Maillot, and F. Bouchet. Crack initiation under thermal fatigue: An overview of CEA experience. part I: Thermal fatigue appears to be more damaging than uniaxial isothermal fatigue. *International Journal of Fatigue*, 31(3):587–600, 2009. doi:10.1016/j.ijfatigue.2008.03.038.

[8] T. Frondelius, M. Haataja, and H. Tienhaara. History of structural analysis & dynamics of Wärtsilä medium speed engines. *Rakenteiden Mekaniikka (Journal of Structural Mechanics)*, 51(2):1–31, 2018. doi:10.23998/rm.69735.

[9] G. Chen, Y. Hu, S. Yan, J. Zhu, L. Yang, and Z. Dong. Failure analysis of a natural gas engine exhaust manifold. *Engineering Failure Analysis*, 154:107660, 2023. doi:10.1016/j.engfailanal.2023.107660.

[10] B. Li, Y. Cui, Y. Fu, K. Deng, Y. Tian, and S. Liu. Marine diesel exhaust manifold failure and life prediction under high-temperature vibration. *Proceedings of the Institution of Mechanical Engineers, Part C: Journal of Mechanical Engineering Science*, 236(11):6180–6191, 2022. doi:10.1177/09544062211064957.

[11] S. Kreivi, T. Kuivaniemi, A. Mäntylä, J. Vaara, J. Istolahti, P. Halla-aho, A. Vuotikka, and T. Frondelius. Feasibility and optimization of a bush-cut aluminium bronze big end bearing: a simulation-based study. *Rakenteiden Mekaniikka*, 56(4):179–198, 2023. doi:10.23998/rm.132039.

[12] Y. Shokrollahi, M.M. Nikahd, K. Gholami, and G. Azamirad. Deep learning techniques for predicting stress fields in composite materials: A superior alternative to finite element analysis. *Journal of Composites Science*, 7(8), 2023. doi:10.3390/jcs7080311.

[13] W.Z. Zhuang and N.S. Swansson. *Thermo-mechanical fatigue life prediction: A critical review*. DSTO Aeronautical and Maritime Research Laboratory Melbourne, VIC, Canada, 1998.

[14] S. Kalluri. Multiaxial and thermomechanical fatigue of materials: A historical perspective and some future challenges. In *ASTM National Symposium on Fatigue and Fracture Mechanics*, number GRC-E-DAA-TN11855, 2013.

[15] B. Salehnasab, J. Marzbanrad, and E. Poursaeidi. Transient thermal fatigue crack propagation prediction in a gas turbine component. *Engineering Failure Analysis*, 130:105781, 2021. doi:10.1016/j.engfailanal.2021.105781.

[16] A. Leppänen, A. Kumpula, J. Vaara, M. Cattarinussi, J. Könnö, and T. Frondelius. Thermomechanical fatigue analysis of cylinder head. *Rakenteiden mekaniikka*, 50(3):179–182, 2017. open access. doi:10.23998/rm.64743.

[17] H. Zhang, G. Liang, X. Qiao, Z. Lyu, L. Li, G. Zhang, and Y. Cui. Experimental and numerical study of inelastic behavior based on simulated cylinder head specimen under thermal cycling conditions. *Journal of the Brazilian Society of Mechanical Sciences and Engineering*, 44(8):372, 2022. doi:10.1007/s40430-022-03652-2.

[18] M. Lorenzini, S.G. Barbieri, V. Mangeruga, and M. Giacopini. Development of an experimental/numerical validation methodology for the design of exhaust manifolds of high performance internal combustion engines. *Engineering Failure Analysis*, 152:107526, 2023. doi:10.1016/j.engfailanal.2023.107526.

[19] M. Chen, Y. Wang, W. Wu, and J. Xin. Design of the exhaust manifold of a turbo charged gasoline engine based on a transient thermal mechanical analysis approach. *SAE Int. J. Engines*, 8(1):75–81, 2015. doi:10.4271/2014-01-2882.

[20] Dassault Systêmes. SIMULIA User Assistance 2023 – Abaqus. URL: https://help.3ds.com/2023/English/DSSIMULIA_Established/SIMULIA_Established_FrontmatterMap/sim-r-DSDocAbaqus.htm?contextscope=all&id=911fcdfb25bd4de980bfe93649a3e257, 2023. Accessed: 16 August 2024.

[21] Dassault Systêmes. SIMULIA User Assistance 2023 – fe-safe. URL: https://help.3ds.com/2023/english/dssimulia_established/SIMULIA_Established_FrontmatterMap/sim-c-DSDocFesafe.htm?contextscope=all&id=4339da8b72ca4ff3b8509399be0bd39c, 2023. Accessed: 16 August 2024.

[22] J.C. Han and L.M. Wright. *Analytical Heat Transfer*. Taylor & Francis, 2022.

[23] SFS-EN 1563:2018. Founding. Spheroidal graphite cast irons. Standard, Finnish Standards Association, 2018.

[24] A. Koivuvaara. Termisesti ja mekaanisesti kuormitettujen komponenttien väsyminen. Master's thesis, University of Oulu, 2024. URL: https://urn.fi/URN:NBN:fi:oulu-202406194734.

[25] C. Bleicher, J. Niewiadomski, A. Kansy, and H. Kaufmann. High-silicon nodular cast iron for lightweight optimized wind energy components. *International Journal of Offshore and Polar Engineering*, 32:201–209, 2022. doi:10.17736/ijope.2022.et06.

[26] A. Ince. A mean stress correction model for tensile and compressive mean stress fatigue loadings. *Fatigue & Fracture of Engineering Materials & Structures*, 40:939–948, 2017. doi:10.1111/ffe.12553.

[27] A. Vepsäläinen, J. Pitkänen, and T. Hyppänen. *Fundamentals of heat transfer*. Lappeenranta University of Technology, 2012. ISBN: 978-952-265-127-3.

[28] J.C. Butcher. *Numerical methods for ordinary differential equations*. Wiley, 2008. ISBN: 9780470753750.

[29] J.S. Téllez-Martínez, M.Z. Sánchez-Hernández, M.J. Vega-Flores, A.A. Pintor-Estrada, H.E. Alva-Medrano, and N.D. Herrera-Sandoval. Analysis of a fundamental procedure for solving the inverse heat conduction problem applied to simple systems. In H Muhammad Ali and T.M. Indra Mahlia, editors, *Heat transfer - Advances in Fundamentals and Applications*, chapter 1. IntechOpen, Rijeka, 2023. URL: https://doi.org/10.5772/intechopen.113133.

[30] Y. Zhang and T. Lu. Unsteady-state thermal stress and thermal deformation analysis for a pressurizer surge line subjected to thermal stratification based on a coupled CFD-FEM method. *Annals of Nuclear Energy*, 108:253–267, 2017. doi:10.1016/j.anucene.2017.04.034.

Sami Kreivi, Janne Kemppainen, Antti-Jussi Vuotikka
Simulation & Calculation, Global Boiler Works Oy
Lumijoentie 8, 90400 Oulu, Finland
firstname.lastname@gbw.fi

Teemu Kuivaniemi, Tero Frondelius
R&D and Engineering, Wärtsilä
Teollisuuskatu 9b, 65170 Vaasa, Finland
firstname.lastname@wartsila.com

Tero Frondelius
Materials and Mechanical Engineering, University of Oulu
Pentti Kaiteran katu 1, 90014 Oulu, Finland
firstname.lastname@oulu.fi